

This is an Open Access document downloaded from ORCA, Cardiff University's institutional repository:<https://orca.cardiff.ac.uk/id/eprint/144823/>

This is the author's version of a work that was submitted to / accepted for publication.

Citation for final published version:

De Marco, Riccardo, Ronen, Itamar, Branzoli, Francesca, Amato, Marisa, Asllani, Iris, Alessandro, Colasanti, Harrison, Neil A. and Cercignani, Mara 2022. Diffusion-weighted MR Spectroscopy (DW-MRS) is sensitive to LPS-induced changes in glial morphometry: a preliminary study. *Brain, Behavior, and Immunity* 99 , pp. 256-265. 10.1016/j.bbi.2021.10.005

Publishers page: <https://doi.org/10.1016/j.bbi.2021.10.005>

Please note:

Changes made as a result of publishing processes such as copy-editing, formatting and page numbers may not be reflected in this version. For the definitive version of this publication, please refer to the published source. You are advised to consult the publisher's version if you wish to cite this paper.

This version is being made available in accordance with publisher policies. See <http://orca.cf.ac.uk/policies.html> for usage policies. Copyright and moral rights for publications made available in ORCA are retained by the copyright holders.



Diffusion-weighted MR Spectroscopy (DW-MRS) is sensitive to LPS-induced changes in human glial morphometry: A preliminary study

Riccardo De Marco¹, Itamar Ronen², Francesca Branzoli^{3,4}, Marisa Amato¹, Iris Asllani^{1,5},
Alessandro Colasanti¹, Neil A Harrison^{*1,6}, Mara Cercignani^{*1,6}

* Joint senior authors

AFFILIATIONS

1. Department of Neuroscience, Brighton and Sussex Medical School, Brighton, UK

2. C. J. Gorter Center for High Field MRI, Department of Radiology, Leiden University Medical Centre, Leiden, The Netherlands

3. Centre for NeuroImaging Research - CENIR, Brain and Spine Institute - ICM, Paris, France

4. Sorbonne University, Univ Paris 06 UMR S 1127, Inserm U 1127, CNRS UMR 7225, Paris, France

5. Department of Biomedical Engineering, Rochester Institute of Technology, Rochester, New York, USA

6. Cardiff University Brain Research Imaging Centre (CUBRIC), Cardiff University, Cardiff, UK

CORRESPONDING AUTHOR: cercignanim@cardiff.ac.uk

WORDS COUNTS: Manuscript (5357 words), Figures: 5, Tables: 2

KEY WORDS: Depression, diffusion MRS, Inflammation, LPS, Microglia, Neuroinflammation

ABSTRACT

Background: Low-dose lipopolysaccharide (LPS) is a well-established experimental method for inducing systemic inflammation and shown by microscopy to activate microglia in rodents. Currently, techniques for in-vivo imaging of glia in humans are limited to TSPO (Translocator protein) PET, which is expensive, methodologically challenging, and has poor cellular specificity. DW-MRS sensitizes MR spectra to diffusion of intracellular metabolites, potentially providing cell-specific information about cellular morphology. In this preliminary study, we applied DW-MRS to measure changes in the apparent diffusion coefficients (ADC) of glial and neuronal metabolites to healthy participants who underwent an LPS administration protocol. We hypothesized that the ADC of glial metabolites will be selectively modulated by LPS-induced glial activation. **Methods:** Seven healthy male volunteers, (mean 25.3 ± 5.9 years) were each tested in two separate sessions once after LPS (1ng/Kg iv) and once after placebo (saline). Physiological responses were monitored during each session and serial blood samples and Profile of Mood States (POMS) completed to quantify white blood cell (WBC), cytokine and mood responses. DW-MRS data were acquired 5-5½ hours after injection from two brain regions: grey matter in the left thalamus, and frontal white matter. **Results:** Body temperature, heart rate, WBC and inflammatory cytokines were significantly higher in the LPS compared to the placebo condition ($p < 0.001$). The ADC of the glial metabolite choline (tCho) was also significantly increased after LPS administration compared to placebo ($p=0.008$) in the thalamus which scaled with LPS-induced changes in POMS total and negative mood (Adj $R^2=0.83$; $p=0.004$). **Conclusions:** DW-MRS may be a powerful new tool sensitive to glial cytomorphological changes in grey matter induced by systemic inflammation.

INTRODUCTION

Effects of systemic inflammation on the brain are implicated in the etiology of a range of common mental illnesses and neurodegenerative disorders (Khandaker et al., 2021). Multiple parallel neural and humoral immune-brain communicatory pathways have been identified, though the ultimate mediator of central effects is increasingly recognized to be microglia (Critchley and Harrison, 2013), brain specialized macrophages which constitute ~10-15% of all brain parenchymal cells. In rodents, peripheral immune challenges, typically using a gram-negative bacterial endotoxin such as lipopolysaccharide (LPS), increase blood brain-barrier permeability (Clawson et al., 1966; Varatharaj and Galea, 2017). It also rapidly triggers a shift in microglial morphometry from a 'resting' to an 'activated' phenotype which is accompanied by an increase in proinflammatory cytokine release (Savage et al., 2019). Though, inter-species sensitivity differs markedly (up to many orders of magnitude), LPS-induced changes in microglial morphometry are also observed in rodents at doses that are broadly species equivalent to those used in human studies. In rodents, these inflammation-induced changes in microglial morphology and secretory profile can be quantified ex-vivo using microscopy, immunohistochemistry, and single cell transcriptomics, and in-vivo using multi-photon imaging through a cranial window (Savage et al., 2019).

In humans, in-vivo methods for imaging microglia are currently limited to Positron Emission Tomography (PET) using tracers that bind to Translocator protein (TSPO), which is overexpressed on the outer mitochondria membrane of activated microglia. TSPO-PET has been used to demonstrate widespread increases in grey matter TSPO binding 3-5 hours after inflammatory challenge (using LPS) in humans (Sandiego et al., 2015) and 4-6 hours in non-human primates (Hannestad et al., 2012). However, TSPO PET is an invasive procedure, involves exposure to radioactivity and TSPO is also expressed in other glial cells as well as on

endothelium. Furthermore, precise quantification of the TSPO PET signal in the brain is substantially complicated by LPS-induced redistribution of TSPO radiotracers across compartments (Yoder et al., 2015) limiting its more widespread use in research and its potential as a viable clinical tool (Schubert et al., 2021). MRI based approaches have been used to index effects of systemic inflammation on brain functional reactivity (functional MRI: fMRI), functional connectivity (resting state fMRI: rs-fMRI), neurochemistry (magnetic resonance spectroscopy: MRS) and microstructure (quantitative magnetization transfer: qMT and diffusion weighted: DW-MRI). While these approaches have highlighted a matrix of brain regions sensitive to peripheral inflammation (Critchley and Harrison, 2013; Garcia-Hernandez et al., 2020; Kraynak et al., 2018), they cannot directly inform on the likely cellular substrates underpinning these inflammation-related changes.

Diffusion-weighted MRS (DW-MRS) offers the potential to address these shortcomings. Briefly, DW-MRI has high sensitivity to tissue microstructure and water compartmentalization (Pierpaoli and Basser, 1996). However, its cellular specificity is limited, as water diffuses similarly through all cell types as well as the extra-cellular environment. In contrast, MRS probes the signal from metabolites, which are predominantly intra-cellular, and in some cases cell-specific. Of the commonly measured metabolites, N-Acetyl-Aspartate (NAA) is exclusively confined within neurons, total creatine (creatine + phosphocreatine = tCr) is found in each brain cell type, while choline compounds (Choline, phosphocholine and glycerophosphocholine = tCho) predominantly reside in glial cells (with a ~3-fold higher concentration than in neurons), O-2A progenitor cells and meningeal cells (Urenjak et al., 1993). The specificity of DW-MRI to different cell types can thus be dramatically improved by combining it with MRS, enabling the morphological properties of specific cell types to be

probed by measuring the apparent diffusion coefficient (ADC) of different metabolites (Ingo et al., 2018; Palombo et al., 2018).

In line with this, DW-MRS has been shown to be sensitive to cell-specific metabolite diffusion changes in the brain occurring in chronic inflammatory conditions. For example, in the cuprizone model of multiple sclerosis, apparent diffusion of both tCho and myo-inositol was observed after 6 weeks of cuprizone with these changes showing moderate to strong correlations with histological measures of microglial and astrocytic area fractions respectively (Genovese et al., 2021b). In humans, patients with systemic lupus erythematosus (SLE) exhibit increased intracellular diffusion of total creatine and total choline in the white matter compared with healthy controls (Ercan et al., 2016). Diffusion of tCr and tCho has also been found to be increased in the primary motor cortex of patients with amyotrophic lateral sclerosis (ALS), suggesting the presence of reactive glia (Reischauer et al., 2018). Data from the thalamic grey matter of multiple sclerosis (MS) patients has shown a decrease in ADC(NAA), which is believed to reflect accompanying neuronal-axonal loss or mitochondrial dysfunction, and a decrease in ADC(tCr), thought to reflect impaired cell energy metabolism (Bodini et al., 2018).

Here we employed DW-MRS to assess the effect of peripherally administered LPS on the ADC of NAA, tCr and tCho within a grey and a white matter region of interest in healthy humans. The thalamus was used as it is an homogeneous grey matter (GM) region known to have among the highest microglial density in human brain (based on TSPO PET) (Schubert et al., 2021) and to be susceptible to peripheral LPS (Buttini et al., 1996). The corona radiata, which is a homogenous white matter (WM) region with relatively low microglial density and reactivity to LPS in humans (Sandiego et al., 2015) (based on TSPO PET) was selected as a control region with low expected signal. Of note, though white matter inflammatory responses are a

feature of some inflammatory models (e.g. Cuprizone) this is not the case with LPS (Hannestad et al., 2012). LPS is a cell-wall component of Gram-negative bacteria. It triggers innate immune activation through the Toll-like receptor 4 (TLR-4) signaling cascade (Chow et al., 1999) and is a well-established method for eliciting systemic inflammation in both animals and humans (Lasselin et al., 2020). In healthy humans, intravenous injection leads to a rapid, dose-dependent increase in circulating white blood cells (particularly neutrophils) and release of proinflammatory cytokines such as tumor necrosis factor- α (TNF- α) and interleukin-6 (IL-6), which are accompanied by raised body temperature and heart rate (Fullerton et al., 2016; van Deventer et al., 1990). It also reliably elicits transient sickness behaviors (that resemble depressive symptoms), facilitating investigation of how regional changes in brain microstructure may perturb behavior and potentially contribute to depression (Dowlati et al., 2010).

MATERIALS AND METHODS

Participants: Seven healthy male subjects (mean age: 25.2 ± 5.9 (std) years, mean body weight: 80.6 ± 10.3 (std) Kg, mean BMI: 24.6 ± 1.7 (std) Kg/m²) were recruited through public advertisement. All were screened to exclude any underlying neurological or psychiatric condition, including substance misuse. All participants were medication free. At screening, participants underwent physical examination and blood samples were taken for full blood count, differential white blood cell (WBC) count (neutrophils, lymphocytes, monocytes, eosinophils, basophils) as well as renal, thyroid, and liver function. Volunteers were asked to abstain from alcohol for 24h before the start of each session. The study was approved by the London-Queen Square Research Ethics Committee (REF 17/LO/0936), and all participants provided written informed consent.

Study Design: We adopted a randomized, double-blind, crossover, repeated measure experimental study design. All participants received an intravenous injection of either LPS (1ng/Kg) prepared from *Escherichia coli* O:113 (U.S. Standard Reference Endotoxin, manufactured for the Clinical Center, NIH) or saline (placebo control) in random order in two separate study sessions spaced a minimum of 2 weeks apart (mean(\pm std) 3.7 ± 3.8 weeks). Three participants received placebo in the first session and four LPS. Participants' systolic and diastolic blood pressure, body temperature and heart-rate were monitored throughout each 8-hour testing session. Blood samples were collected at baseline and at 3 and 6 hours post injection to measure differential WBC count. A DW-MRS scanning session was scheduled for 5-5½ hours after each injection. This timing was informed by: 1) prior human and baboon TSPO PET studies that report increased TSPO uptake at 3-5 and 4-6 hours post LPS respectively as well as sustained subjective sickness and systemic inflammatory responses at this time-point confirming an ongoing peripheral and central inflammatory response. 2) Evidence from prior human studies using 1ng/kg LPS that show a significant reduction in peripheral limb and joint discomfort coupled with less pronounced pyrexia at this timepoint meaning that participants would be better able to comply with requirements to remain very still during the DW-MRS scanning session (which is highly sensitive to motion).

Cytokine Analyses: Blood drawn into purple top (EDTA) BD Vacutainer tubes (Becton, Dickson and Company, Franklin Lakes, New Jersey, United States) was centrifuged at 2000 rpm for 20 min, then plasma removed, aliquoted, and frozen at -80 °C. Plasma (IL-6), tumor necrosis factor- α (TNF- α) and interleukin (IL-10) were measured using Quantikine® High Sensitivity ELISA kits for IL-6 (R&D Systems inc., Minneapolis, United States). Limits of detection were 0.031 pg/mL, 0.022 pg/mL and 0.09 pg/mL respectively and intra- and inter-assay coefficients of variation were 6.9% and 9.6% (IL-6), 2.2% and 6.7% (TNF- α) and 9.3%

and 13.1% (IL-10). For the IL-10 analyses, 5 samples measured below the lowest standard and a value of one-half of the lower limit of detection was assigned to these samples (Breen et al., 2011). All samples were tested in duplicate. Values were natural log transformed before analysis.

Behavioral Analyses: Participants completed self-rating questionnaires at baseline then at 5 further time-points after each injection (1, 2, 3, 4 and 6 hours post injection) to assess LPS-induced mood changes. These included: profile of mood states (POMS), fatigue visual analogue scale (fVAS) and the Karolinska Sickness Questionnaire (Andreasson et al., 2018).

DWMRS acquisition and analysis: MRI and MRS were obtained at 3T (Siemens Magnetom Prisma, Siemens Healthineers, Erlangen, Germany). After a standard localizer, a T1-weighted magnetization prepared rapid acquisition gradient echo (TR=1900 ms; TE=3.97 ms; TI=904 ms, flip angle=8 deg, FOV 220 × 220 mm², matrix size 192 × 192) was acquired in sagittal orientation and reconstructed in 3 orthogonal planes. These high-resolution scans were used to position two 4.5 cm³ DW-MRS volumes of interest (VOIs) on the left thalamus and left corona radiata. VOIs were chosen based on prior data indicating high microglial density and reactivity to LPS in thalamus and low microglial density and LPS reactivity in corona radiata (Schubert et al., 2021; Sandiego et al., 2015; Buttoni et al., 1996). The left hemisphere was chosen as it is more commonly implicated in inflammation-induced cognitive changes (Haroon et al., 2014; Harrison et al., 2015). The DW-MRS sequence used was a bipolar sequence based on a semi-Localization by Adiabatic SElective Refocusings (semi-LASER) sequence (Genovese et al., 2021a) with TE=100ms, TR=5s, spectral width=2500 kHz, number of complex points=1024. The following diffusion weighting conditions were used: one at b=0 s/mm² and three at b=3823 s/mm² with diffusion gradients applied in three orthogonal directions ([1, 1, -0.5], [1, -0.5, 1],

[−0.5, 1, 1] in the VOI coordinate system, diffusion gradient duration=14 ms, diffusion time=50 ms). The number of signals averages (NSA) was 32 for each condition. A short (NSA=4) scan without water suppression was performed for eddy current correction. B₀ shimming was performed using a fast automatic shimming technique with echo-planar signal trains utilizing mapping along projections, FAST (EST) MAP (Gruetter and Tkáč, 2000).

The spectra were transferred off-line for analysis with customized software implemented in Matlab (Mathworks, Natick MA, USA). Spectral analyses were performed with linear prediction singular value decomposition (LPSVD), and the peak area estimates for the three orthogonal gradient directions at high b value were averaged and the resulting mean values were used to compute the ADC values for the three metabolites. The operator was blind to participant condition (i.e. LPS or placebo). The spectra at b=0 s/mm² were used to estimate relative tCho and tNAA (tNAA = NAA + NAAglutamate) concentrations, expressed as the ratio between their peak area to the tCr peak area.

Statistical Analysis: Analyses was conducted using SPSS statistics 24. Physiological, cytokine and behavioral effects of LPS were analyzed using repeated-measures factorial ANOVAs (factors: treatment (LPS, placebo), time (pre injection, post injection as described)) with significant effects followed up with paired sample t-tests. The ADC of the three metabolites as well as the tCho and tNAA concentration relative to tCr ([tCho]/[tCr] and [tNAA]/[tCr]) were compared between sessions (LPS vs placebo) using a paired-sample t-test. Associations between changes in ADC(tCho) and changes in mood (POMS), temperature and peripheral immune measures (cell counts and cytokines) were assessed using Pearson's correlation coefficient.

RESULTS

Physiological effects: Effects of LPS on physiological parameters are summarized in **Figure**

1. Significant condition (LPS/Placebo) \times time interactions were observed for body temperature ($F_{(13,78)}=21.6$, $p<0.001$) and heart rate ($F_{(13,78)}=8.48$, $p<0.001$). LPS significantly increased body temperature, from 60 minutes, peaking at 3 hours post injection, and significantly increased heart rate which peaked between 2 and 4 hours post-injection. Significant condition (LPS/Placebo) \times time interactions were also observed for total WBC count ($F_{(2,12)}=30.6$, $p<0.001$) as well as for each differential WBC count (Neutrophils: $F_{(2,12)}=54.9$, $p<0.001$; lymphocytes: $F_{(2,12)}=26.2$, $p<0.001$; monocytes: $F_{(2,12)}=23.7$, $p<0.001$) with the greatest changes observed at 6 hours. Post-LPS cell count increases at 6 hours (compared to baseline) were: $113 \pm 14.5\%$ and $230.6 \pm 32.3\%$ for Total WBC and Neutrophils respectively. Lymphocytes showed the opposite pattern: $-54.9 \pm 6.1\%$ at 6hr (relative to baseline) while monocytes displayed a $-60.9 \pm 8.2\%$ decrease at 3 hrs after LPS followed by a $51.4 \pm 11.6\%$ increase at 6 Hrs after LPS (both relative to baseline) (Table 1) consistent with results reported in other LPS challenge studies (Peters van Ton et al., 2021).

Cytokine levels: LPS induced significant increases in circulating cytokines shown by significant condition (LPS/Placebo) \times time (baseline, 6 hours) interactions for IL-6: $F_{(1,6)}=14.91$, $p=0.008$; TNF- α : $F_{(1,6)}=50.05$, $p<0.001$; and IL-10 $F_{(1,6)}=27.67$, $p=0.002$ (**Figure 2**).

Behavioral response: LPS injection led to significant temporary changes in mood, fatigue, and sickness symptoms as shown by POMS questionnaire, fVAS, and sickness questionnaire. Specifically, LPS was associated with a reduction in total mood score: main effect of condition ($F_{(1,6)}=77.73$, $p<0.001$), condition \times time interaction ($F_{(5,30)}=2.31$, $p=0.068$) and increase in

negative mood score: main effect of condition ($F_{(1,6)}=57.17$, $p<0.001$), condition \times time interaction ($F_{(5,30)}=2.38$, $p=0.062$) (**Figure 3** Insets). LPS induced changes in both total mood and negative mood scores (compared to placebo) peaked 1 hour post injection (paired-sample t-tests: $t_{(6)}=3.6$, $p=0.011$; $t_{(6)}=-3.0$, $p=0.024$) respectively (**Figure 3** Insets). Moreover, LPS induced a significant increase in both fatigue: significant condition \times time interaction for fVAS ($F_{(5,20)}=4.06$, $p=0.01$) and sickness score ($F_{(5,25)}=6.34$, $p=0.001$). fVAS showed a rapid increase in fatigue that peaked at 1 hour post LPS injection, compared to baseline (paired-sample t-test $t_{(6)}=-3.6$, $p=0.011$) while sickness score peaked at 2 hours ($t_{(6)}=-5.5$, $p=0.002$) followed by a gradual improvement.

DW-MRS: Main effects of LPS: The spectra were of good quality for all participants. As an example, **Figure 4** shows spectra acquired in the thalamus of the same participant in the two conditions (placebo and LPS). The average ADCs of tNAA, tCr and tCho are shown in **Table 2**; the between-condition difference in metabolite ADC is shown in **Figure 5**. Paired t-test revealed a significant increase in ADC(tCho) in the thalamus for the LPS compared to the placebo condition ($t_{(6)}=-3.9$, $p=0.008$), (ADC(tCho) (Thalamus): placebo ($M=1.26 \times 10^{-4}$, $SD=3 \times 10^{-5}$), LPS ($M=1.76 \times 10^{-4}$, $SD=1.6 \times 10^{-5}$)). No significant difference was detected in ADC(tCho) in the WM control region between the two conditions. ADC(tNAA) and ADC(tCr) did not differ significantly between conditions in either VOI. No significant differences in the metabolites' relative concentration (expressed as $[tCho]/[tCr]$ and $[tNAA]/[tCr]$) were observed in either region between conditions. There was no significant correlation between LPS-induced changes in body temperature and ADCs for any of the metabolites (all $p>0.1$). Exploratory analyses investigating associations between ADCs and peripheral immune measures revealed a trend association between LPS-induced changes in thalamic ADC(tCho)

and associated change in monocyte count at 6 hours (Adj $R^2=0.46$; $p=0.09$). All other associations were non-significant ($p>0.1$).

Correlation between mood deterioration and ADC(tCho) change: To investigate potential associations between mood change and putative changes in neuroinflammation we regressed peak change in mood (1 hour post injection minus baseline) for LPS compared to placebo against changes in the ADC(tCho) between conditions. LPS-associated changes in both POMS total and negative mood were significantly associated with changes in ADC(tCho) of the thalamus (Adj $R^2=0.79$; $p=0.007$ and Adj $R^2=0.83$; $p=0.004$, respectively) (**Figure 3**).

DISCUSSION

Glial activation is a hallmark of the neuroinflammatory cascade and a pathological feature of a wide range of severe and disabling central nervous system (CNS) diseases. Increased density, altered morphology, and/or a pro-inflammatory immune phenotype of microglia and astrocytes are consistent post-mortem findings in autoimmune neuroinflammatory disorders, such as MS or Neuro SLE, and neurodegenerative diseases such as ALS and Alzheimer's disease (González-Reyes et al., 2017; McGeer and McGeer, 2002; Perry and Holmes, 2014). Furthermore, post-mortem and neuroimaging evidence of alterations in microglia and astrocytes in depression and schizophrenia have implicated glia in the neuropathology of psychiatric disorders that are linked to heightened systemic inflammation (Almeida et al., 2020; Dantzer et al., 2008; Lanquillon et al., 2000; Najjar et al., 2013). At a systemic level, increasing evidence has linked the onset of depression with raised circulating inflammatory markers (Dowlati et al., 2010; Osimo et al., 2020). Yet, the exact mechanisms underlying the brain response to systemic inflammation remain elusive as sensitive and viable neuroimaging

methods for the *in vivo* assessment of glial response to systemic inflammation are yet to be fully developed.

Here using DW-MRS, we report results from 7 healthy subjects providing preliminary evidence for altered intracellular metabolite diffusion in the context of experimentally induced systemic inflammation in humans. Changes of metabolite diffusion properties have been considered to mirror cytomorphological cell rearrangement or, in a pathological framework, tissue damage. The primary finding of this study is the increased ADC(tCho) in the gray matter after LPS injection compared to placebo. This result suggests that cytomorphological changes in glial cells observed using microscopy in rodents and baboons after systemic inflammation can also be detected in-vivo in humans using DW-MRS. This finding is also in keeping with recent DW-MRS results in rodents showing an increase in tCho and myo-inositol ADCs using the Cuprizone model of neuroinflammation, which correspondingly correlate with induced changes in microglial and astrocytic area fraction recorded histologically (Genovese et al., 2021b), as well as in human neurological diseases, such as neuropsychiatric systemic lupus erythematosus (Ercan et al., 2016) and ALS (Reischauer et al., 2018), that are each characterized by glial activation. However, confirmation of our preliminary findings will require future replication in larger studies.

The absence of a significant change in the neuronal marker tNAA ADC in our current study is also consistent with histological studies which indicate no effect of LPS on neuronal morphology. However, it is worth stressing that our small sample size may have meant we were under powered to detect diffusion changes in other metabolites. Of note, reductions in ADC(tNAA) have been previously reported in MS, however this finding was interpreted as reflecting accompanying neuronal damage or cell loss which is a feature of this model but not

systemic LPS (Bodini et al., 2018). A potential bias in our experiment was the effect of LPS on body temperature and consequently metabolite diffusion. However, the absence of an effect of LPS on diffusion of the neuronal marker tNAA in either VOI or on tCho in our WM control region, coupled with an absence of even a trend level association between changes in body temperature and any of the metabolite ADCs suggests this an unlikely cause of our findings.

Though tCho has only limited specificity to glial cells, its significant ADC change following LPS compared to placebo is consistent with previous studies reporting microglial and astrocytic neuroinflammatory responses following peripheral LPS exposure in mice (Ryu et al., 2019). The activation of central inflammation has also been reported in humans using TSPO PET where it has been proposed to be mediated mainly by microglial cells (Sandiego et al., 2015). Microglia are known to be the principal mediator of innate immune responses within the CNS. In the healthy brain, microglial cells are highly dynamic and extend and retract multiple long finger-like processes to monitor their local environment (Nimmerjahn et al., 2005). Changes in brain homeostasis due to infection, injury or neurodegeneration can alter microglia gene expression, morphology and motility (Helmut et al., 2011). However, during neuroinflammation both microglia and astrocytes undergo metabolic, functional and morphological changes (Heneka et al., 2014). In this reactive state glial cells can release neurotoxic factors such as proinflammatory cytokines and reactive nitrogen and oxygen species, ultimately affecting neuronal transmission and neurogenesis (Orihuela et al., 2016). Once activated, microglia display a thickening and retraction of their processes and assume an amoeboid spherical shape with increased cell body size (Davis et al., 1994). In a similar way, reactive astrocytes are characterized by cellular hypertrophy and overlapping processes (Sofroniew and Vinters, 2010). It is therefore uncertain whether the changes in tCho diffusion we observed stemmed from microglial or astrocytic activation. However, in a mouse model of

astrocytic hypertrophy myo-inositol diffusion changes were sensitive to cytomorphological rearrangement, whereas tCho was unaffected (Ligneul et al., 2019). Similarly, in the cuprizone model mentioned earlier, induced changes in tCho scaled with histological changes in microglia and myo-inositol with changes in astrocytes (Genovese et al., 2021b).

It is worth noting that we were unable to quantify myo-inositol diffusion using our current method. The higher diffusivity of tCho we observed is also consistent with the increased intracellular space that characterizes microglia in the activated state. Furthermore, although microglial and astrocytic activation are both key components of neuroimmune processes, microglia are thought to initiate the process triggered by LPS and then causally induce astrocytic activation (Liddel et al., 2017). In line with this finding, a DW-MRI study using a multi-compartment tissue model based on microglia and astrocyte cell shape has recently shown typical microglial changes at 8 hrs post LPS injection in rodents with a subsequent astrocytic signal emerging later at 24 hrs (Garcia-Hernandez et al., 2020). This time-dependent neuroimmune cascade allows us to speculate that the observed increase in tCho value may selectively reflect microglial activation. In support of this, since the tCho concentration was unchanged between sessions it is unlikely that the observed change in ADC was influenced by infiltrating or peri-vascular immune cells.

A second finding from our study was the tight correlation between LPS-induced changes in thalamic ADC(tCho) and the severity of induced mood changes. Despite being characterized by a high density of microglial cells, the thalamus has not previously been reported as a key structure for the psychological and behavioral effects associated with systemic inflammation (Harrison, 2017). Instead, previous fMRI studies have reported functional changes of the subgenual cingulate and amygdala (Davies et al., 2020; Harrison et al., 2009) following

immune challenges which correlate with the severity of mood/ depressive changes. Decreased global functional connectivity has also emerged as a putative neurobiological underpinning of mood deterioration driven by peripheral inflammation (Dipasquale et al., 2016). This later finding suggests a potentially widespread effect of systemic inflammation on grey matter which is consistent with the widespread increase in TSPO expression previously reported following LPS injection in both baboons and humans (Hannestad et al., 2012) (Sandiego et al., 2015). Hence, the effect that we report within the thalamus (which was selected based on its high microglial density and sensitivity to LPS rather than a specific role in mood processing) is likely a proxy of more general glial morphological changes in the brain grey matter. Given the time implications of acquiring data in multiple VOIs we restricted this preliminary study to acquisition of data in a single grey and white matter volume of interest. Nevertheless, it will be important for future studies to consider data acquisition from a greater range of VOIs to further address the specificity of regional changes to discrete behavioral features.

As discussed above, the main limitation of our study is the relatively modest sample size and consequently the need to replicate our findings in future larger studies. Another limitation is that our data were only acquired at a single time-point (5-5½ hours) after LPS/placebo injection. Though human LPS studies typically only scan at a single time point it will be important for future studies to begin to address the temporal evolution of brain changes and their association with the evolution/ resolution of specific behavioral and cellular features. Following LPS changes in physiological e.g. heart-rate, temperature, cytokine and sickness symptoms typically peak 2-3 hours post administration. However, cellular responses e.g. neutrophil and monocyte counts typically continue to increase up until at least 6 hours post injection. TSPO PET studies indicate central (brain) glial activation 3-5 hours after LPS in humans (Sandiego et al., 2015) and from 1-3 hours in baboons rising further at 4-6 hours before returning to (or below) baseline at 22-24 hours (Hannestad et al., 2012). Thus, though many

indices of peripheral immune responses peak relatively early, central glial responses appear to peak later and remain evident until at least 6 hours post-LPS. How and when these initial pro-inflammatory responses ultimately resolve and how they relate to acute and potentially more persistent symptoms in some participants will need to be addressed in future studies. Rodent studies combining longitudinal DW-MRS with histological analyses will also be valuable in clarifying the cell-specific basis of the signal we report.

DW-MRS is a challenging measurement, and several sources of errors need to be addressed at both the acquisition and processing stages. Motion occurring during the diffusion time has a significant effect on the DW-MRS signal. More specifically, simple linear translational motion results in a constant signal phase shift that can be corrected in the post-acquisition stage, when individual shots are acquired separately, resulting in no significant effect on the calculated metabolite ADC. Rotational and compressive motion, resulting for example from cardiac pulsation, causes a non-constant phase shift across the VOI that results in drop in signal intensity (Anderson and Gore, 1994). This type of error cannot be corrected, and if individual acquisitions during which such signal drop occurred are included in the signal average, the resulting ADC is significantly overestimated. These acquisitions must be excluded, and in our post-processing pipeline we do so using a simple criterion imposed on the amplitude of the NAA peak (the strongest peak in the spectrum), taking into account the expected variance of the peak amplitude across acquisitions based on the variance of the noise (Genovese et al., 2021a).

DW-MRS also suffers from low signal-to-noise ratio (SNR), compared to a simple MRS acquisition: the need to accommodate the diffusion gradients within the sequence dictates a longer echo time than standard “Short-TE” MRS sequences, and the need to acquire several

diffusion weighted conditions limits the number of averages that is possible to acquire during a given scan time. SNR affects the variance in metabolite ADC values in a non-linear fashion that can be estimated via calculation of error propagation in the estimation of ADC with the assumption of mono-exponential decay (Ronen and Valette, 2015). Even when the b factor is optimally set to be roughly $1/\text{ADC}$, the error propagation is significant and amplifies the variance in metabolite ADC values several times above that of the non-diffusion weighted MRS signal. A robustness/reproducibility study for single volume DW-MRS (Wood et al., 2015) indicates that with carefully optimized acquisition and processing DW-MRS protocols as the one we applied in this study, it is possible to reach the required statistical power for detecting ADC differences in case-control studies similar to the one presented here.

Finally, the clear physical responses to LPS mean that both the participant and the researcher will become aware of allocation to the LPS condition ~ 1 hour after its administration (though notably not all participants receiving placebo in the first session realized this until completing the second LPS session). Nevertheless, it is important to note that critically the DW-MRS data were analyzed completely blind to condition.

To conclude, we present a novel MR imaging paradigm that could enable the quantification of glial morphological changes in-vivo in humans. Although resident immunocompetent cells have emerged as a central component in a wide array of brain disorders, a gold standard method to selectively assess different biological mechanisms in vivo is still lacking. TSPO PET has been widely used to quantify neuroinflammation. However, it is invasive, expensive, requires the use of radioactivity and remains challenging to quantify without an arterial input function, particularly in conditions where inflammation is not restricted to the CNS (Nettis et al., 2020). Unlike PET, DW-MRS has the advantage of being non-invasive and it can be acquired with

other routine MRI images. A limitation is that it can currently only be acquired in pre-specified VOIs rather than whole brain. Nevertheless, pending further validation in larger studies DW-MRS could form a valuable tool for investigating neuroinflammatory processes in clinical populations and for providing evidence of target engagement for novel pharmacotherapies being developed to target glial cells.

ACKNOWLEDGEMENTS

We are grateful to the National Institute of Health Clinical Centre (NIHCC), Bethesda, Maryland, US for supplying the GMP grade LPS used in this study. FB acknowledges the support of the programs 'Institut des neurosciences translationnelle' [ANR-10-IAIHU-06] and 'Infrastructure d'avenir en Biologie Santé' [ANR-11-INBS-0006]. This study was also part funded by an MRC Confidence in Concept Grant awarded to the University of Sussex. The authors would like to thank Dr. Edward J. Auerbach, and Prof. Małgorzata Marjańska for implementing the DW-MRS sequence on the Siemens platform.

REFERENCES

- Almeida, P.G.C., Nani, J.V., Oses, J.P., Brietzke, E., Hayashi, M.A.F., 2020. Neuroinflammation and glial cell activation in mental disorders. *Brain, Behav. Immun. - Heal.* 2, 100034. <https://doi.org/10.1016/j.bbih.2019.100034>
- Anderson, A.W., Gore, J.C., 1994. Analysis and correction of motion artifacts in diffusion weighted imaging. *Magn. Reson. Med.* 32, 379–387. <https://doi.org/10.1002/mrm.1910320313>
- Andreasson, A., Wicksell, R.K., Lodin, K., Karshikoff, B., Axelsson, J., Lekander, M., 2018. A global measure of sickness behaviour: Development of the Sickness Questionnaire. *J.*

459 Health Psychol. 23, 1452–1463. <https://doi.org/10.1177/1359105316659917>

460 Bodini, B., Branzoli, F., Poirion, E., García-Lorenzo, D., Didier, M., Maillart, E., Socha, J.,
 461 Bera, G., Lubetzki, C., Ronen, I., Lehericy, S., Stankoff, B., 2018. Dysregulation of
 462 energy metabolism in multiple sclerosis measured in vivo with diffusion-weighted
 463 spectroscopy. *Mult. Scler. J.* 24, 313–321. <https://doi.org/10.1177/1352458517698249>

464 Breen, E.C., Reynolds, S.M., Cox, C., Jacobson, L.P., Magpantay, L., Mulder, C.B., Dibben,
 465 O., Margolick, J.B., Bream, J.H., Sambrano, E., Martínez-Maza, O., Sinclair, E., Borrow,
 466 P., Landay, A.L., Rinaldo, C.R., Norris, P.J., 2011. Multisite Comparison of High-
 467 Sensitivity Multiplex Cytokine Assays. *Clin. Vaccine Immunol.* 18, 1229.
 468 <https://doi.org/10.1128/CVI.05032-11>

469 Buttini, M., Limonta, S., Boddeke, H.W.G.M., 1996. Peripheral administration of
 470 lipopolysaccharide induces activation of microglial cells in rat brain. *Neurochem. Int.* 29,
 471 25–35. [https://doi.org/10.1016/0197-0186\(95\)00141-7](https://doi.org/10.1016/0197-0186(95)00141-7)

472 Carlyle Clawson, C., Francis Hartmann, J., Vernier, R.L., 1966. Electron microscopy of the
 473 effect of gram-negative endotoxin on the blood-brain barrier. *J. Comp. Neurol.* 127, 183–
 474 197. <https://doi.org/10.1002/cne.901270204>

475 Chow, J.C., Young, D.W., Golenbock, D.T., Christ, W.J., Gusovsky, F., 1999. Toll-like
 476 receptor-4 mediates lipopolysaccharide-induced signal transduction. *J. Biol. Chem.* 274,
 477 10689–10692. <https://doi.org/10.1074/jbc.274.16.10689>

478 Critchley, H.D., Harrison, N.A., 2013. Visceral Influences on Brain and Behavior. *Neuron.*
 479 <https://doi.org/10.1016/j.neuron.2013.02.008>

480 Dantzer, R., O'Connor, J.C., Freund, G.G., Johnson, R.W., Kelley, K.W., 2008. From
 481 inflammation to sickness and depression: When the immune system subjugates the brain.

482 Nat. Rev. Neurosci. 9, 46–56. <https://doi.org/10.1098/rspa.2008.0233>

483 Davies, K.A., Cooper, E., Voon, V., Tibble, J., Cercignani, M., Harrison, N.A., 2020.
 484 Interferon and anti-TNF therapies differentially modulate amygdala reactivity which
 485 predicts associated bidirectional changes in depressive symptoms. *Mol. Psychiatry* 1–11.
 486 <https://doi.org/10.1038/s41380-020-0790-9>

487 Davis, E.J., Foster, T.D., Thomas, W.E., 1994. Cellular forms and functions of brain microglia.
 488 *Brain Res. Bull.* [https://doi.org/10.1016/0361-9230\(94\)90189-9](https://doi.org/10.1016/0361-9230(94)90189-9)

489 Dipasquale, O., Cooper, E.A., Tibble, J., Voon, V., Baglio, F., Baselli, G., Cercignani, M.,
 490 Harrison, N.A., 2016. Interferon- α acutely impairs whole-brain functional connectivity
 491 network architecture – A preliminary study. *Brain. Behav. Immun.* 58, 31–39.
 492 <https://doi.org/10.1016/j.bbi.2015.12.011>

493 Dowlati, Y., Herrmann, N., Swardfager, W., Liu, H., Sham, L., Reim, E.K., Lancôt, K.L.,
 494 2010. A Meta-Analysis of Cytokines in Major Depression. *Biol. Psychiatry* 67, 446–457.
 495 <https://doi.org/10.1016/j.biopsych.2009.09.033>

496 Ercan, E., Magro-Checa, C., Valabregue, R., Branzoli, F., Wood, E.T., Steup-Beekman, G.M.,
 497 Webb, A.G., Huizinga, T.W.J., van Buchem, M.A., Ronen, I., 2016. Glial and axonal
 498 changes in systemic lupus erythematosus measured with diffusion of intracellular
 499 metabolites. *Brain* 139, 1447–57. <https://doi.org/10.1093/brain/aww031>

500 Fullerton, J.N., Segre, E., De Maeyer, R.P., Maini, A.A., Gilroy, D.W., 2016. Intravenous
 501 Endotoxin Challenge in Healthy Humans: An Experimental Platform to Investigate and
 502 Modulate Systemic Inflammation. *J. Vis. Exp* 53913. <https://doi.org/10.3791/53913>

503 Garcia-Hernandez, R., Carpena, A.T., Drakesmith, M., Koller, K., Jones, D.K., Canals, S.,
 504 Santis, S. De, 2020. Imaging Microglia and Astrocytes non-invasively using Diffusion

505 MRI. bioRxiv 2020.02.07.938910. <https://doi.org/10.1101/2020.02.07.938910>

506 Genovese, G., Marjańska, M., Auerbach, E.J., Cherif, L.Y., Ronen, I., Lehericy, S., Branzoli,
507 F., 2021a. In vivo diffusion-weighted MRS using semi-LASER in the human brain at 3 T:
508 Methodological aspects and clinical feasibility. *NMR Biomed.* 34.
509 <https://doi.org/10.1002/NBM.4206>

510 Genovese, G., Palombo, M., Santin, M.D., Valette, J., Ligneul, C., Aigrot, M.S., Abdoukader,
511 N., Langui, D., Millecamps, A., Baron-Van Evercooren, A., Stankoff, B., Lehericy, S.,
512 Petiet, A., Branzoli, F., 2021b. Inflammation-driven glial alterations in the cuprizone
513 mouse model probed with diffusion-weighted magnetic resonance spectroscopy at 11.7
514 T. *NMR Biomed.* <https://doi.org/10.1002/nbm.4480>

515 González-Reyes, R.E., Nava-Mesa, M.O., Vargas-Sánchez, K., Ariza-Salamanca, D., Mora-
516 Muñoz, L., 2017. Involvement of astrocytes in Alzheimer's disease from a
517 neuroinflammatory and oxidative stress perspective. *Front. Mol. Neurosci.*
518 <https://doi.org/10.3389/fnmol.2017.00427>

519 Gruetter, R., Tkáč, I., 2000. Field Mapping Without Reference Scan Using Asymmetric Echo-
520 Planar Techniques.

521 Hannestad, J., Gallezot, J.-D., Schafbauer, T., Lim, K., Kloczynski, T., Morris, E.D., Carson,
522 R.E., Ding, Y.-S., Cosgrove, K., 2012. Endotoxin-Induced Systemic Inflammation
523 Activates Microglia: [11 C]PBR28 Positron Emission Tomography in Nonhuman
524 Primates. *Neuroimage* 63, 232–239. <https://doi.org/10.1016/j.neuroimage.2012.06.055>

525 Haroon, E., Woolwine, B.J., Chen, X., Pace, T.W., Parekh, S., Spivey, J.R., Hu, X.P., Miller,
526 A.H., 2014. IFN-alpha-induced cortical and subcortical glutamate changes assessed by
527 magnetic resonance spectroscopy. *Neuropsychopharmacology* 39, 1777–1785.

528 <https://doi.org/10.1038/npp.2014.25>

529 Harrison, N.A., 2017. Brain structures implicated in inflammation-associated depression, in:

530 Current Topics in Behavioral Neurosciences. Springer Verlag, pp. 221–248.

531 https://doi.org/10.1007/7854_2016_30

532 Harrison, N.A., Brydon, L., Walker, C., Gray, M.A., Steptoe, A., Critchley, H.D., 2009.

533 Inflammation Causes Mood Changes Through Alterations in Subgenual Cingulate

534 Activity and Mesolimbic Connectivity. *Biol. Psychiatry* 66, 407–414.

535 <https://doi.org/10.1016/j.biopsych.2009.03.015>

536 Harrison, N.A., Cooper, E., Dowell, N.G., Keramida, G., Voon, V., Critchley, H.D.,

537 Cercignani, M., 2015. Quantitative magnetization transfer imaging as a biomarker for

538 effects of Systemic inflammation on the brain. *Biol. Psychiatry* 78, 49–57.

539 <https://doi.org/10.1016/j.biopsych.2014.09.023>

540 Helmut, K., Hanisch, U.K., Noda, M., Verkhratsky, A., 2011. Physiology of microglia. *Physiol.*

541 Rev. 91, 461–553. <https://doi.org/10.1152/physrev.00011.2010>

542 Heneka, M.T., Kummer, M.P., Latz, E., 2014. Innate immune activation in neurodegenerative

543 disease. *Nat. Rev. Immunol.* <https://doi.org/10.1038/nri3705>

544 Ingo, C., Brink, W., Ercan, E., Webb, A.G., Ronen, I., 2018. Studying neurons and glia non-

545 invasively via anomalous subdiffusion of intracellular metabolites. *Brain Struct. Funct.*

546 223, 3841–3854. <https://doi.org/10.1007/s00429-018-1719-9>

547 Khandaker, G., Harrison, N., Bullmore, E., Dantzer, R. (Eds.), 2021. Textbook of

548 Immunopsychiatry. Cambridge University Press. <https://doi.org/10.1017/9781108539623>

549 Kraynak, T.E., Marsland, A.L., Wager, T.D., Gianaros, P.J., 2018. Functional neuroanatomy

550 of peripheral inflammatory physiology: A meta-analysis of human neuroimaging studies.
 551 *Neurosci. Biobehav. Rev.* <https://doi.org/10.1016/j.neubiorev.2018.07.013>

552 Lanquillon, S., Krieg, J.C., Bening-Abu-Shach, U., Vedder, H., 2000. Cytokine production and
 553 treatment response in major depressive disorder. *Neuropsychopharmacology* 22, 370–
 554 379. [https://doi.org/10.1016/S0893-133X\(99\)00134-7](https://doi.org/10.1016/S0893-133X(99)00134-7)

555 Lasselin, J., Lekander, M., Benson, S., Schedlowski, M., Engler, H., 2020. Sick for science:
 556 experimental endotoxemia as a translational tool to develop and test new therapies for
 557 inflammation-associated depression. *Mol. Psychiatry*. [https://doi.org/10.1038/s41380-](https://doi.org/10.1038/s41380-020-00869-2)
 558 020-00869-2

559 Liddel, S.A., Gattenplan, K.A., Clarke, L.E., Bennett, F.C., Bohlen, C.J., Schirmer, L.,
 560 Bennett, M.L., Münch, A.E., Chung, W.S., Peterson, T.C., Wilton, D.K., Frouin, A.,
 561 Napier, B.A., Panicker, N., Kumar, M., Buckwalter, M.S., Rowitch, D.H., Dawson, V.L.,
 562 Dawson, T.M., Stevens, B., Barres, B.A., 2017. Neurotoxic reactive astrocytes are
 563 induced by activated microglia. *Nature* 541, 481–487.
 564 <https://doi.org/10.1038/nature21029>

565 Ligneul, C., Palombo, M., Hernández-Garzón, E., Carrillo-de Sauvage, M.A., Flament, J.,
 566 Hantraye, P., Brouillet, E., Bonvento, G., Escartin, C., Valette, J., 2019. Diffusion-
 567 weighted magnetic resonance spectroscopy enables cell-specific monitoring of astrocyte
 568 reactivity in vivo. *Neuroimage* 191, 457–469.
 569 <https://doi.org/10.1016/j.neuroimage.2019.02.046>

570 McGeer, P.L., McGeer, E.G., 2002. Inflammatory processes in amyotrophic lateral sclerosis.
 571 *Muscle and Nerve*. <https://doi.org/10.1002/mus.10191>

572 Najjar, S., Pearlman, D.M., Alper, K., Najjar, A., Devinsky, O., 2013. Neuroinflammation and

573 psychiatric illness. *J. Neuroinflammation*. <https://doi.org/10.1186/1742-2094-10-43>

574 Nettis, M.A., Veronese, M., Nikkheslat, N., Mariani, N., Lombardo, G., Sforzini, L., Enache,
575 D., Harrison, N.A., Turkheimer, F.E., Mondelli, V., Pariante, C.M., 2020. PET imaging
576 shows no changes in TSPO brain density after IFN- α immune challenge in healthy human
577 volunteers. *Transl. Psychiatry* 10, 1–11. <https://doi.org/10.1038/s41398-020-0768-z>

578 Nimmerjahn, A., Kirchhoff, F., Helmchen, F., 2005. Resting Microglial Cells Are Highly
579 Dynamic Surveillants of Brain Parenchyma in Vivo 308, 1314–1319.

580 Orihuela, R., McPherson, C.A., Harry, G.J., 2016. Microglial M1/M2 polarization and
581 metabolic states. *Br. J. Pharmacol.* 173, 649–665. <https://doi.org/10.1111/bph.13139>

582 Osimo, E.F., Pillinger, T., Rodriguez, I.M., Khandaker, G.M., Pariante, C.M., Howes, O.D.,
583 2020. Inflammatory markers in depression: A meta-analysis of mean differences and
584 variability in 5,166 patients and 5,083 controls. *Brain. Behav. Immun.*
585 <https://doi.org/10.1016/j.bbi.2020.02.010>

586 Palombo, M., Shemesh, N., Ronen, I., Valette, J., 2018. Insights into brain microstructure from
587 in vivo DW-MRS. *Neuroimage*. <https://doi.org/10.1016/j.neuroimage.2017.11.028>

588 Perry, V.H., Holmes, C., 2014. Microglial priming in neurodegenerative disease. *Nat. Rev.*
589 *Neurol.* <https://doi.org/10.1038/nrneurol.2014.38>

590 Peters van Ton, A.M., Leijte, G.P., Franssen, G.M., Bruse, N., Booi, J., Doorduyn, J.,
591 Rijpkema, M., Kox, M., Abdo, W.F., Pickkers, P., 2021. Human in vivo neuroimaging to
592 detect reprogramming of the cerebral immune response following repeated systemic
593 inflammation. *Brain. Behav. Immun.* <https://doi.org/10.1016/j.bbi.2021.04.004>

594 Pierpaoli, C., Basser, P.J., 1996. Toward a Quantitative Assessment of Diffusion Anisotropy.

595 Reischauer, C., Gutzeit, A., Neuwirth, C., Fuchs, A., Sartoretti-Schefer, S., Weber, M., Czell,
 596 D., 2018. In-vivo evaluation of neuronal and glial changes in amyotrophic lateral sclerosis
 597 with diffusion tensor spectroscopy. *NeuroImage Clin.* 20, 993–1000.
 598 <https://doi.org/10.1016/j.nicl.2018.10.001>

599 Ronen, I., Valette, J., 2015. Diffusion-Weighted Magnetic Resonance Spectroscopy. *eMagRes*
 600 4, 733–750. <https://doi.org/10.1002/9780470034590.EMRSTM1471>

601 Ryu, K.Y., Lee, H.J., Woo, H., Kang, R.J., Han, K.M., Park, H.H., Lee, S.M., Lee, J.Y., Jeong,
 602 Y.J., Nam, H.W., Nam, Y., Hoe, H.S., 2019. Dasatinib regulates LPS-induced microglial
 603 and astrocytic neuroinflammatory responses by inhibiting AKT/STAT3 signaling. *J.*
 604 *Neuroinflammation* 16, 190. <https://doi.org/10.1186/s12974-019-1561-x>

605 Sandiego, C.M., Gallezot, J.-D., Pittman, B., Nabulsi, N., Lim, K., Lin, S.-F., Matuskey, D.,
 606 Lee, J.-Y., O'Connor, K.C., Huang, Y., Carson, R.E., Hannestad, J., Cosgrove, K.P.,
 607 2015. Imaging robust microglial activation after lipopolysaccharide administration in
 608 humans with PET. *Proc. Natl. Acad. Sci.* 112, 12468–12473.
 609 <https://doi.org/10.1073/PNAS.1511003112>

610 Savage, J.C., St-Pierre, M.-K., Hui, C.W., Tremblay, M.-E., 2019. Microglial Ultrastructure in
 611 the Hippocampus of a Lipopolysaccharide-Induced Sickness Mouse Model. *Front.*
 612 *Neurosci.* 13, 1340. <https://doi.org/10.3389/fnins.2019.01340>

613 Schubert, J., Tonietto, M., Turkheimer, F., Zanotti-Fregonara, P., Veronese, M., 2021.
 614 Supervised clustering for TSPO PET imaging. *Eur. J. Nucl. Med. Mol. Imaging* 1–12.
 615 <https://doi.org/10.1007/s00259-021-05309-z>

616 Sofroniew, M. V., Vinters, H. V., 2010. Astrocytes: Biology and pathology. *Acta Neuropathol.*
 617 <https://doi.org/10.1007/s00401-009-0619-8>

618 Urenjak, J., Williams, S.R., Gadian, D.G., Noble, M., 1993. Proton Nuclear Magnetic
619 Resonance Spectroscopy Unambiguously Identifies Different Neural Cell Types.

620 van Deventer, S.J.H., Büller, H.R., ten Cate, J.W., Aarden, L.A., Hack, C.E., Sturk, A., 1990.
621 Experimental Endotoxemia in Humans: Analysis of Cytokine Release and Coagulation,
622 Fibrinolytic, and Complement Pathways. *Blood* 76, 2520–2526.
623 [https://doi.org/https://doi.org/10.1182/blood.V76.12.2520.2520](https://doi.org/10.1182/blood.V76.12.2520.2520)

624 Varatharaj, A., Galea, I., 2017. The blood-brain barrier in systemic inflammation. *Brain*.
625 *Behav. Immun.* <https://doi.org/10.1016/j.bbi.2016.03.010>

626 Wood, E.T., Ercan, A.E., Branzoli, F., Webb, A., Sati, P., Reich, D.S., Ronen, I., 2015.
627 Reproducibility and optimization of in vivo human diffusion-weighted MRS of the corpus
628 callosum at 3T and 7T. *NMR Biomed.* 28, 976. <https://doi.org/10.1002/NBM.3340>

629 Yoder, K.K., Territo, P.R., Hutchins, G.D., Hannestad, J., Morris, E.D., Gallezot, J.D.,
630 Normandin, M.D., Cosgrove, K.P., 2015. Comparison of standardized uptake values with
631 volume of distribution for quantitation of [¹¹C]PBR28 brain uptake. *Nucl. Med. Biol.* 42,
632 305–308. <https://doi.org/10.1016/j.nucmedbio.2014.11.003>

633 TABLE LEGENDS

634 Table 1: Effects of LPS on white blood cell count

635 Data represent mean ± standard error

636

637 Table 2: effects of LPS on glial metabolites ADC

638 Data represent mean ± standard error

639 FIGURE LEGENDS

Figure 1: Effect of LPS on vital signs and WCC

A) Body temperature. B) Blood pressure. C) WCC. D) Heart rate. Red lines represent LPS condition, blue lines placebo. X Axis shows hours post LPS or Placebo injection. Significance values show Treatment \times sample contrasts with baseline (* $p < 0.05$ ** $p < 0.001$).

Figure 2: Effect of LPS on cytokines levels

Changes (mean \pm SE) in plasma levels (natural log transformed) of circulating cytokines (* $p < 0.05$ ** $p < 0.001$). Significance values were tested with paired sample t-tests.

Figure 3: Effect of LPS on mood and relationship with ADC(tCho) change

Correlation between ADC(tCho) change between the two sessions and the difference between mood changes from baseline to 1 Hr post injection in the two session. (A) POMS total mood score, (B) POMS negative mood score. Insets show the mood score throughout the two sessions; grey shaded areas indicate the two timepoints used to obtain the POMS difference correlated with the ADC(tCho) change.

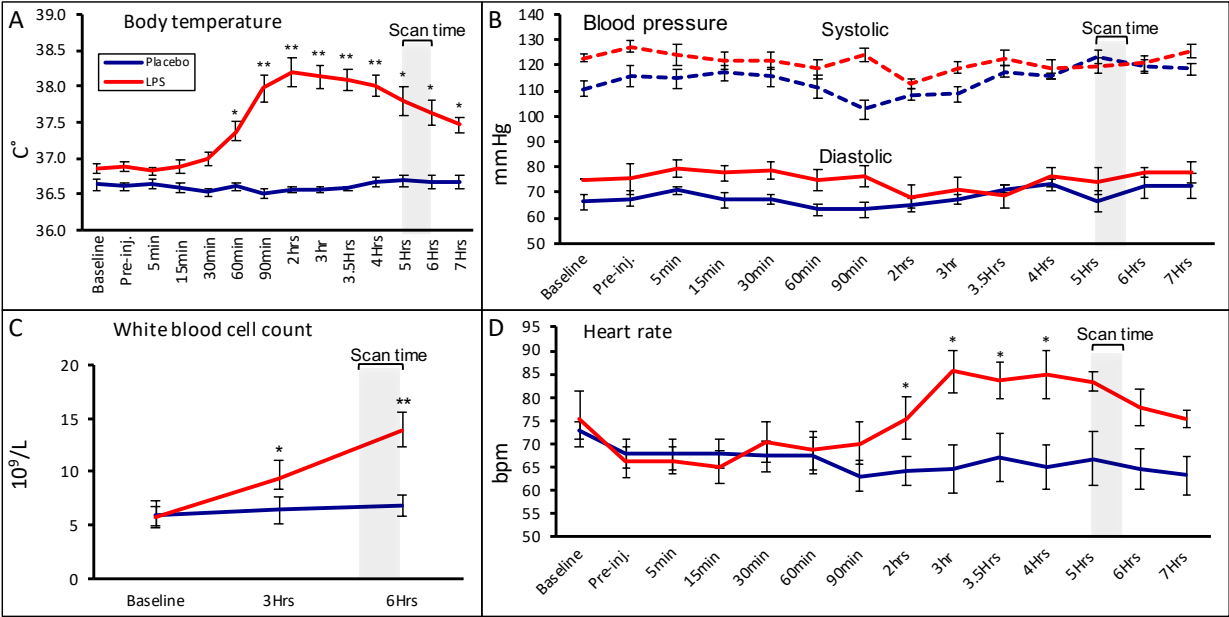
Figure 4: MR Spectra

Example of MR spectra acquired at $b = 0 \text{ s/mm}^2$ and $b = 3823 \text{ s/mm}^2$ in the left thalamus of one subject after placebo (top) and LPS (bottom) injections.

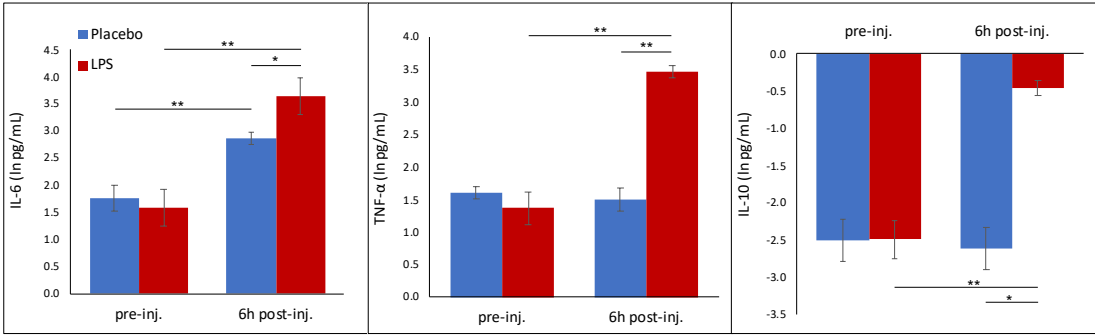
Figure 5: Metabolites ADC responses to LPS

tCho, tCr and tNAA ADC differences between LPS and placebo sessions in thalamus (A) and white matter (C). Mean differences and standard deviations are reported. Volumes of interest (VOIs) were located in the thalamus (B) and in the parietal white matter (corona radiata) (D). P-value relates to comparison between LPS and placebo session.

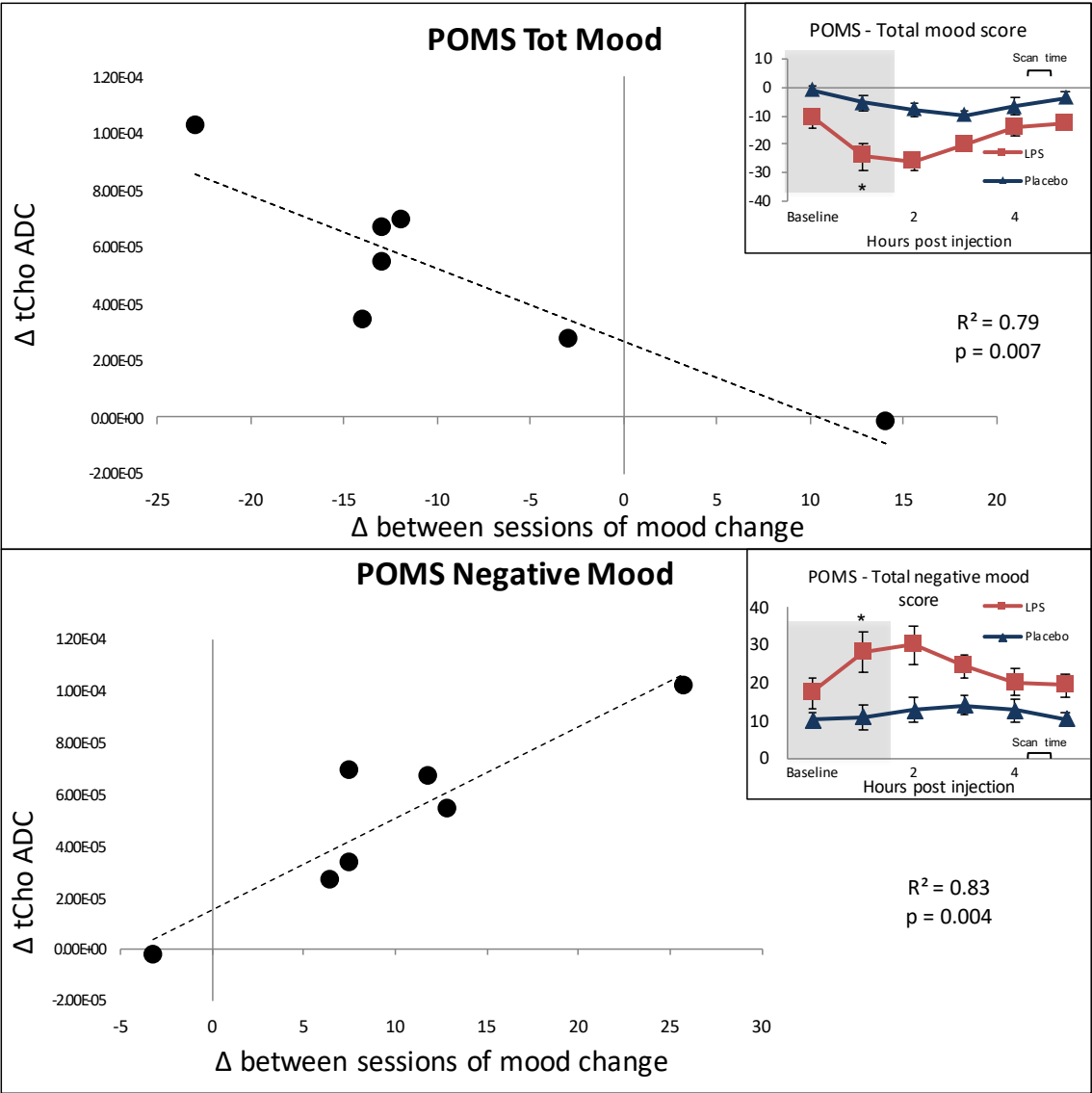
665 **Figure 1: Effect of LPS on vital signs and WCC**



668 **Figure 2: Effect of LPS on cytokine levels**



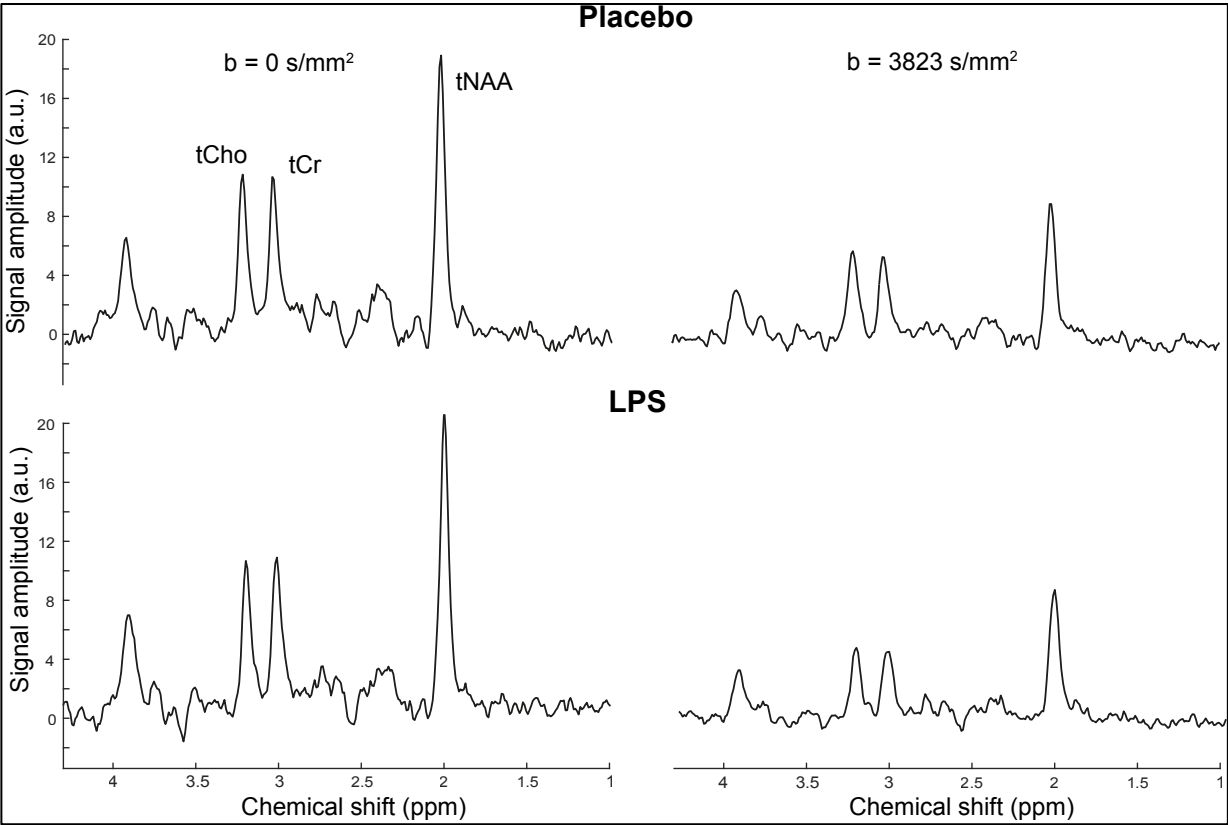
671 **Figure 3: Effect of LPS on mood and relationship with tCho ADC change**



672

673

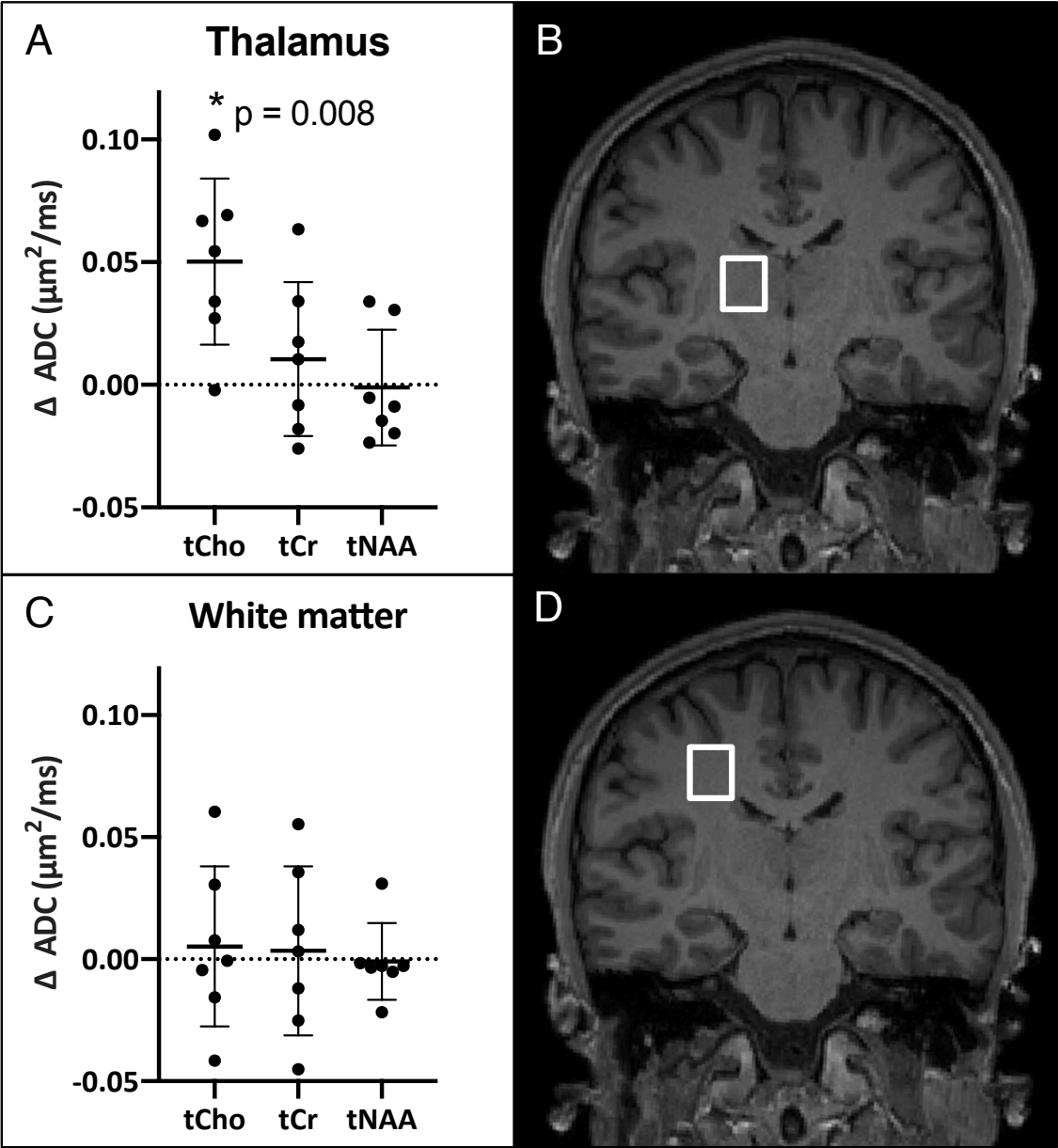
674 **Figure 4: MR Spectra**



675

676

677 **Figure 5: Metabolites ADC responses to LPS**



678

679